Journal of Colloid and Interface Science 677 (2025) 293–302

Contents lists available at ScienceDirect

Journal of Colloid And Interface Science

journal homepage: www.elsevier.com/locate/jcis

Regular Article

Lipidic drug delivery systems are responsive to the human microbiome

Jonathan Caukwell [a,b], Salvatore Assenza [c,d,e], Karl A. Hassan [b], Brett A. Neilan [b], Andrew J. Clulow [f,g], Livia Salvati Manni [a,f,h,*], Wye-Khay Fong [a,b,*]

[a] School of Chemistry, Monash University, Clayton 3800, VIC, Australia
[b] School of Environmental and Life Sciences, University of Newcastle, Callaghan 2308, NSW, Australia
[c] Departamento de Física Teórica de la Materia Condensada, Universidad Autónoma de Madrid, E-28049 Madrid, Spain
[d] Condensed Matter Physics Center (IFIMAC), Universidad Autónoma de Madrid, E-28049 Madrid, Spain
[e] Instituto Nicolás Cabrera, Universidad Autónoma de Madrid, E-28049 Madrid, Spain
[f] Australian Synchrotron, ANSTO, 800 Blackburn Road, Clayton, VIC 3168, Australia
[g] Drug Delivery, Disposition & Dynamics, Monash Institute of Pharmaceutical Sciences, 381 Royal Parade, Parkville, VIC 3052, Australia
[h] School of Chemistry and University of Sydney Nano Institute, The University of Sydney, NSW 2006, Australia

GRAPHICAL ABSTRACT

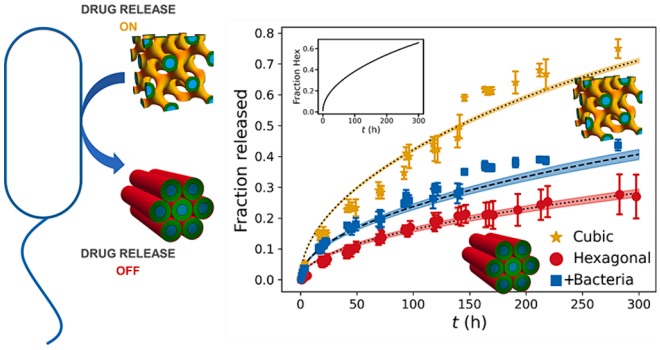

ARTICLE INFO

Keywords:
Monoolein
Lipid-cubic phase
Lipid mesophase
Drug delivery systems
Nano-biome interactions
Microbiome
Nanomaterials
Nanotherapeutics
Response to physiological stimuli

ABSTRACT

In vitro and *in vivo* tests for therapeutic agents are typically conducted in sterile environments, but many target areas for drug delivery are home to thousands of microbial species. Here, we examine the behaviour of lipidic nanomaterials after exposure to representative strains of four bacterial species found in the gastrointestinal tract and skin. Small angle X-ray scattering measurements show that the nanostructure of monoolein cubic and inverse hexagonal phases are transformed, respectively, into inverse hexagonal and inverse micellar cubic phases upon exposure to a strain of live *Staphylococcus aureus* often present on skin and mucosa. Further investigation demonstrates that enzymatic hydrolysis and cell membrane lipid transfer are both likely responsible for this effect. The structural responses to *S. aureus* are rapid and significantly reduce the rate of drug release from monoolein-based nanomaterials. These findings are the first to demonstrate how a key species in the live human microbiome can trigger changes in the structure and drug release properties of lipidic nanomaterials. The effect

Abbreviations: GI, Gastrointestinal; SAXS, Small angle X-ray scattering; V_2, Reverse bicontinuous cubic phase; H_2, Inverse hexagonal phase; I_2, Inverse micellar cubic phase; Lα, Lamellar; MO, Monoolein; OA, Oleic acid; EV, Extracellular vesicle; OD, Optical density.

* Corresponding authors at: School of Chemistry, Monash University, Clayton 3800, VIC, Australia.
E-mail addresses: salvatil@ansto.gov.au (L. Salvati Manni), khay.fong@monash.edu (W.-K. Fong).

https://doi.org/10.1016/j.jcis.2024.07.216
Received 6 June 2024; Received in revised form 15 July 2024; Accepted 27 July 2024
Available online 8 August 2024

appears to be strain specific, varies from patient to patient and body region to body region, and is anticipated to affect the bioapplication of monoglyceride-based formulations.

1. Introduction

To date, the development of nanomaterials for drug delivery applications has focused on the optimisation of drug-loading capacity, ease of functionalisation, and stimuli-responsive drug release properties [1,2]. Recent studies have analysed the interaction between these nanomaterials and biological fluids, unveiling mechanisms that are critical for the design of 'smart' nano-therapeutics including cellular trafficking dynamics and protein corona formation [3,4]. However, even though our bodies are covered in ecological communities of symbiotic bacteria – inside and out – there is a paucity of knowledge on how nanomaterials behave when exposed to these microorganisms. Several hundred grams of live bacteria reside in the gastrointestinal (GI) tract at any one time and suppositories and tablets cannot avoid exposure to these bacteria [5]. Similarly, transdermal patches and other topical formulations are placed in direct contact with the skin microbiota. These microbial communities have only recently been characterised in terms of their diversity, function, and role in health and disease [6]. Moreover, the human microbiome plays a vital role in human health; it is implicated in many biological processes: harvesting energy, strengthening tissue integrity, protecting against pathogens, regulating host immunity, and vitamin biosynthesis [7,8]. Gut bacteria metabolise and bioaccumulate drugs before host absorption, in turn affecting drug absorption, efficacy, and side-effect profile [9,10]. This has profound consequences for the success of pharmaceutical treatments. In this work, we focus on lipidic nanomaterials and examine the effects that human-associated bacterial species have on their self-assembly and drug release properties.

Non-lamellar lipid mesophases are promising drug delivery systems with complex nanostructures that determine the kinetics of drug release [11]. Hydrophilic drugs can be loaded into the internal aqueous channels; hydrophobic drugs in the hydrophobic domains; and amphiphilic drugs at the interface between these domains (Fig. 1). The marked differences between these domains are key determinants of drug transport, thus ultimately affecting the release rate [12]. The liquid crystalline reverse bicontinuous cubic (V_2) or inverse hexagonal (H_2) nanostructures can be dispersed into solution in the presence of a stabiliser to create cubosomes or hexosomes, respectively [13]. Their unique combination of biocompatibility, stability to dilution, dynamic self-assembled structure, and sustained drug release qualities make lipid mesophases attractive drug delivery vehicles [14–16].

The nanostructure of the lipid mesophase is determined by the shape and packing behaviour of the constituent lipids. The self-organisation of these lipid assemblies is a dynamic process that is influenced by the surrounding environment. Environmental conditions such as pH, temperature, and level of hydration can influence lipid geometry and packing behaviour, thereby affecting the liquid crystalline nanostructure [17]. This sensitivity to the local environment has been manipulated for biosensing applications and stimuli-responsive drug delivery [17]. While this ability can be exploited for 'smart' drug delivery, it could be responsible for unforeseen changes in drug release properties when the lipidic nanomaterials interact with the human microbiome.

The existing literature exploring the interaction of lipidic materials and bacteria is focussed on antimicrobial applications [18–24]. Dyett et al. have observed the fusion of cubosomes with lipid bilayers under flow [25], and more recently, the fusion dynamics with gram-positive and gram-negative bacteria [26]. Their work has demonstrated that the cell envelope structure governs the kinetics of lipidic nanocarrier fusion with the cell. Most cubosomes employed for drug delivery are composed of monoolein (MO), a monoglyceride that can be hydrolysed by enzymatic digestion to create oleic acid (OA) and glycerol [27–30]. Thorn et al. have demonstrated *ex vivo* that a bacterial lipase extracted from an opportunistic human pathogen *Pseudomonas cepacia* accelerated the digestion of MO cubosomes, thereby 'triggering' release of the entrapped hydrophobic drug cargo [22,31]. However, live bacteria can express a number of different lipases – for example, *Malassezia globosa* secretes 13 different types [32]. Further, different species from the same genus secrete lipases with varying amino acid sequences; the activity of each lipase is dramatically influenced by pH, temperature, and metal ions [33]. As such, little is known about the effects of live bacteria in the native microbiome on lipidic drug delivery systems. In this study, the behaviour of MO cubic and hexagonal phases when exposed to live bacteria is examined for the first time with regards to the mechanism and kinetics of these effects and the consequent effect on drug release properties. We have chosen representative bacterial strains of four species that are present within commonly targeted routes of administration to achieve this: *Staphylococcus aureus* (skin/nasal mucosal membranes), *Pseudomonas aeruginosa* (pathogenic), *Escherichia coli*

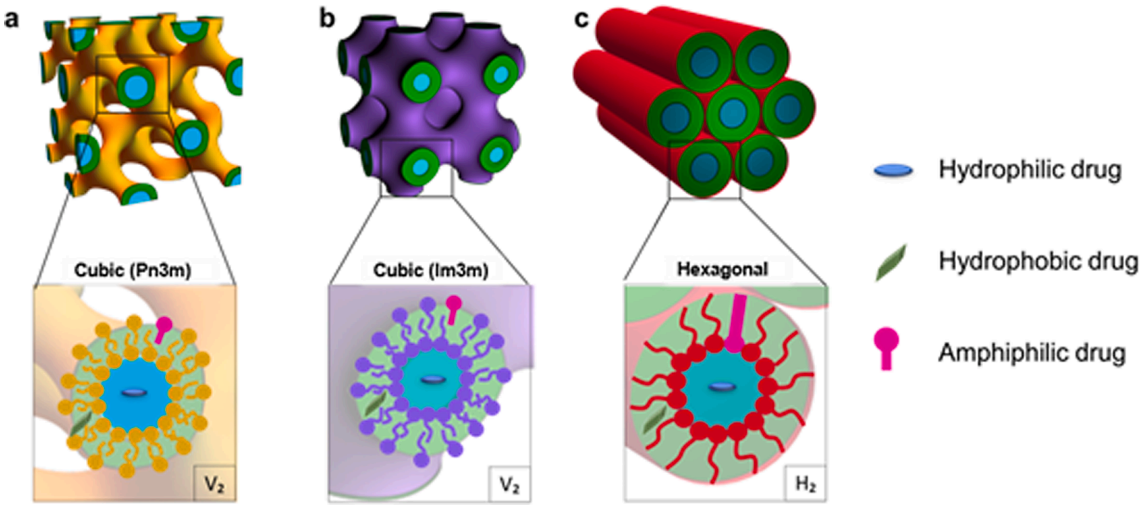

Fig. 1. Non-lamellar lipid mesophases (**a–b**: inverse cubic; **c**: inverse hexagonal). Hydrophilic, lipophilic and amphiphilic drugs can be loaded into the water channels, lipid bilayer, and the interface between them, respectively.

(caecum/colon), and *Lactobacillus rhamnosus* (colon).

2. Materials and methods

2.1. Bacterial subcultures

Lactobacillus rhamnosus (*L. rhamnosus*, ATCC 10863) was a gift from biological sciences; *Escherichia coli* (*E. coli*, NCTC 10418), *Pseudomonas aeruginosa* (*P. aeruginosa*, NCTC 10490), and *Staphylococcus aureus* (*S. aureus*, NCTC 6571) were acquired from the Neilan laboratory; all were stored at −80 °C in 50 % v/v glycerol (Panasonic, MDF-U55V) prior to use. Chloroform and methanol (anhydrous) were purchased from ThermoFischer Scientific (Australia).

De Man, Rogosa and Sharpe (MRS) solid stock media, Mueller-Hinton (MH) solid stock media, and tryptone were purchased from Oxoid (Basingstoke, Hants, UK). NaCl was obtained from ROWE Scientific (Wangara, WA, Australia). Yeast extract was obtained from Sigma Aldrich (St. Louis, MO, USA). Aqueous solutions were prepared using Milli-Q water (Milli-Q IQ 7000, Milli-Q).

All experimental work involving the use of *S. aureus* or *P. aeruginosa* (Biosafety Level 2 organisms) was conducted in a biosafety cabinet (EuroClone, Safemate ECO 1.8). All tools, materials and equipment were purchased sterile or sterilised (autoclave) prior to use. Work was conducted inside a biosafety cabinet or under a Bunsen flame to maintain sterility.

2.1.1. Liquid subculture preparation

E. coli, *P. aeruginosa* and *S. aureus* were grown in Luria Bertani (LB) broth or Mueller-Hinton (MH) media as specified. *L. rhamnosus* was grown in MRS media. Briefly, the appropriate growth media was inoculated with bacterial glycerol stock and incubated overnight at 37 °C with 300 rpm shaking (Eppendorf, ThermoMixer C). The following day, these overnight cultures were diluted in fresh media (1:35), incubated at 37 °C with 300 rpm shaking, and the resulting subcultures used during exponential phase of growth. Bacterial growth was monitored by measuring optical density (OD) at 600 nm and regarded as exponential phase growth after reaching an OD of 1 (Eppendorf, BioSpectrometer fluorescence).

Unless specified otherwise, liquid bacterial subcultures used in all experiments were grown to mid – late exponential growth phase.

2.1.2. Isolation of cell membrane lipids from E. coli

E. coli overnight culture (30 mL) was prepared as previously outlined and used to inoculate 3 L of LB media. This new culture was incubated at 37 °C with 180 rpm shaking until reaching an OD of 1.777. Cells were pelleted by centrifugation (4200 rpm, 45 min), the supernatant discarded, and cells redispersed in 50 mL phosphate buffer (PB) using a vortex mixer (Classic vortex mixer, VELP, Italy). Cells were extracted by centrifugation (15 000 *g*, 5 min, 4 °C) and washed twice with PB.

Cell membrane lipids were isolated from pelleted cells using a modified Bligh and Dyer method [34]. Briefly, cells were dispersed in organic solvent using vortex mixing (2:1 $CHCl_3$:MeOH, v/v), combined with water, and the mixture shaken (5:95:20 cells:organic solvent:H_2O, m:v:v in g & mL, resp.). The mixture was centrifuged (1000*g*, 5 min), the bottom layer was recovered, filtered through cotton wool to remove particulate, and stripped of solvent in vacuo. After the residual solvent was removed using a stream of N_2, the isolated cell membrane lipids were stored at −20 °C under N_2 prior to use.

Glass equipment was used throughout the process to prevent leaching of plastic resins and contamination of the lipid extract.

2.2. Structural characterisation of lipids

2.2.1. SAXS sample preparation

Oleic acid (Technical grade, 90 %), and Pluronic F-127 were purchased from Sigma Aldrich (MO, USA). Dimodan UP/B SG (>99 % monoglycerides) was a gift from Danisco (NSW, Australia). Phosphate buffer (12.8 mM NaCl; 2.7 mM KCl; 10.0 mM Na_2HPO_4; 1.8 mM KH_2PO_4; pH 7.41) was prepared using salts purchased from Rowe Scientific (Minto, Australia). Chloroform and methanol (anhydrous) were purchased from ThermoFischer Scientific (Australia). Tryptone and De Man, Rogosa and Sharpe (MRS) solid stock media were purchased from Oxoid. Yeast extract was obtained from Sigma Aldrich. Aqueous solutions were prepared using Milli-Q water (Milli-Q IQ 7000, Milli-Q).

2.2.1.1. Lipid mesophase gels (bulk phases). The lipid mixture used to prepare the H_2 phases was prepared by dissolving the combined lipids in 9:1 $CHCl_3$:MeOH (v/v) and evaporating the solvent under a stream of N_2. Dimodan was utilised as received for the preparation of V_2 phases. Lipids were stored under N_2 at 4 °C prior to use.

Lipids were first heated in an oven (60 °C) to reduce viscosity and aid transfer. Lipid (24 μL) and liquid bacterial subculture or sterile media (16 μL) were then transferred to separate gas-tight glass syringes (Hamilton, NV, USA) and mixed using a syringe coupler (Formulatrix, OH, USA) as previously reported [35].

2.2.1.2. Structured lipid particles (cubosomes). Formulations for equilibrium studies were prepared by dispersing 10 wt% lipid with 2 wt% Pluronic F-127 stabiliser in the relevant liquid growth media using probe sonication in an icebath (Duty cycle: 2 s on, 1 s off; Power: 50 %; Duration: 10–30 min, Branson Sonifier 450A).

Formulations used in dynamic studies were prepared analogously by dispersing 5 wt% lipid with 0.5 wt% F-127 stabiliser in LB.

Particle size and polydispersity were characterised using dynamic light scattering (DLS) (Zetasizer Nano ZS, Malvern Analytical).

2.2.1.3. Extracted E. Coli cell membrane lipid particles. For dynamic studies of cubosomes interacting with extracted bacterial lipids, the cell lipid formulation was prepared by dispersing 5 wt% isolated cell membrane lipids in phosphate buffer as previously mentioned. Particle size and polydispersity were characterised using DLS.

2.2.2. Analytical methods

2.2.2.1. SAXS sample measurement and analysis

2.2.2.1.1. Equilibrium studies. Lipid mesophase gel samples for equilibrium studies were prepared by loading 40 mg of the lipid mesophase into a quartz capillary, with or without the presence of bacteria in the exponential phase of growth (Supplementary Information). Lipid mesophases were sandwiched between 30 μL of the same aqueous media used for hydration (i.e. sterile liquid growth media or bacterial subculture).

Structured lipid particle samples were prepared in quartz capillaries by combining 40 μL of structured lipid particle dispersion with 40 μL of either liquid growth media or bacteria subculture in the exponential phase of growth. All capillary samples were sealed and incubated overnight (37 °C) prior to SAXS measurement.

2.2.2.1.2. Sample measurement. Equilibrium state small angle X-ray scattering (SAXS) was performed on a point-collimated SAXSess instrument (Cu Kα X-rays; $\lambda = 1.54$ Å, Anton Paar, Graz, Austria) equipped with a Dectris Eiger R 1 M detector (Dectris, Baden-Daettwil, Switzerland) and temperature-controlled stage (±0.1 °C). All measurements were recorded using 1.5 mm quartz capillary tubes (Capillary Tube Supplies Ltd, Cornwall, UK) at 37 °C for 15 min, unless stated otherwise. SAXSAnalysis software (Anton Paar) was used for radial integration of detector images.

2.2.2.1.3. Dynamic study. Dynamic studies were performed on the SAXS/WAXS beamline at the Australian Synchrotron using the sample autoloader [36].

On site, structured lipid particle dispersions and *E. coli* cell lipid dispersions were stored at 37 °C prior to and between measurements.

Samples (100 μL) were loaded into 96-well plates and placed into the autoloader. The instrument was programmed to mix the structured lipid particle dispersions with an equal volume of *E. coli* cell lipid dispersion immediately prior to the first SAXS measurement. The mixed sample was then returned to the well from which it was taken and remeasured 37 min and 133 min after the initial mixing event.

Experiments were performed at 11 keV and 37 °C. Scattering patterns were obtained for 1 s on a Pilatus 2 M detector (Dectris, Switzerland). The in-house analysis software Scatterbrain was used to reduce detector images to plots of intensity *versus* the magnitude of the scattering vector, *q*. The sample – detector distance was calibrated to be 1402 mm using a silver behenate standard at the outset of the measurements.

2.2.2.1.4. Data treatment and analysis. The 2D diffraction patterns recorded by the detector were radially averaged and the scattering intensity, I(q), was plotted as a function of the magnitude of the scattering vector, q, using the respective software. I(q) is denoted as the magnitude of the scattering vector, q:

$$q = \frac{4\pi}{\lambda} sin(\theta) \tag{1}$$

where 2θ is the total scattering angle and λ=1.127 Å. Liquid crystalline phases were identified based on the q spacing of Bragg diffraction peaks [37]: the q spacing ratio $\sqrt{2}:\sqrt{3}:\sqrt{4}:\sqrt{6}:\sqrt{8}:\sqrt{9}\ldots$ is characteristic of the double diamond bicontinuous cubic phase (V_2: Pn3m); the q spacing ratio $\sqrt{2}:\sqrt{4}:\sqrt{6}:\sqrt{8}:\sqrt{10}\ldots$ is characteristic of the primitive bicontinuous cubic phase (V_2: Im3m); the q spacing ratio $1:\sqrt{3}:\sqrt{4}\ldots$ is characteristic of the inverse hexagonal (H_2) phase; the q spacing ratio $\sqrt{3}:\sqrt{8}:\sqrt{11}:\sqrt{12}:\sqrt{16}:\sqrt{19}\ldots\ldots$ is characteristic of the Inverse micellar cubic phase (I_2: Fd3m). Liquid crystalline lattice parameters were calculated based on peak spacings using Eqs. (2) and (3):

V_2 and I_2

$$a = \frac{2\pi}{q}\left(\sqrt{(h^2+k^2+l^2)}\right) \tag{2}$$

H_2

$$a = \frac{4\pi}{q\sqrt{3}}\left(\sqrt{(h^2+hk+k^2)}\right) \tag{3}$$

where a is the lattice parameter, and h, k, l are Miller indices of the lattice plane.

2.2.2.2. pH characterisation. Temperature and pH measurements of liquid growth media and structured lipid particle dispersions were taken at specified time intervals before and after mixing with an equal volume of bacterial subculture and incubating at 37 °C with 300 rpm shaking (HANNA Instruments, HI5221).

2.3. Ultrafiltration of bacterial cultures into fractions

S. aureus and *E. coli* subcultures were prepared from overnight inoculate cultures in sterile MH media as previously outlined. Cells were removed by centrifugation (4000 rpm, 4 °C, 5 min), followed by filtration (0.45 μm pore syringe filter). Cell-free cultures were separated into different size classes and concentrated 70-fold by ultrafiltration (Amicon Ultra Centrifugal Filters, Merck) (4000 rpm, 4 °C, 15 min per cycle). Fractions were diluted with fresh MH media (1:10), mixed with an equal volume of monoolein nanoparticle dispersion, and incubated overnight (37 °C, 240 rpm, 16 h). SAXS was performed on a point-collimated Bruker NanoSTAR instrument (Cu Kα X-rays; λ = 1.54 Å, Bruker, Billerica, USA) equipped with a Vantec-2000 2D detector (Bruker) and temperature-controlled stage (±0.1 °C). All measurements were recorded using 1.5 mm quartz capillary tubes at 37 °C for 15 min, unless stated otherwise.

2.4. Cross-polarized light microscopy

Cross-polarized light microscopy (cPLM) was conducted using a light microscope (Zeiss Axioscop 40) equipped with polarizing filters, temperature-controlled stage (Linkham) and camera (MaoSongtech, China). Monoolein cubic phase gel was prepared (as above) using monoolein and aqueous buffer (sterile or inoculated with *S. aureus*). A sample of each hydrated cubic phase was sandwiched between a glass microscope slide and coverslip. The appropriate aqueous buffer was transferred to the edges of the coverslip and drawn between the slides by capillary action. Three identical slides were made with sterile aqueous buffer, three with buffer inoculated with *S. aureus*, and a slide containing only aqueous buffer inoculated with *S. aureus*. The slides were sealed with 5 min epoxy (Selley's). To gather equilibrium data, each slide was imaged under cross-polarized light at t = 0 and again at t = +17 hr. To gather kinetics data, one slide from the V_2-*S. aureus* test group was placed on a heated microscope stage (37 °C) and imaged under cross-polarized light at 6 min intervals for 17 hr. All other replicates were imaged under broad-field and cross-polarized light before and after incubation at 37 °C for 17 hr. Images were analysed using Image J software.

2.5. Drug release study

2.5.1. Materials

Rhodamine B (>95 %; Sigma Aldrich) was used to prepare a dye stock solution in LB. Cellulose dialysis tubing (14 kDa) was purchased from Sigma Aldrich.

2.5.2. Method

Rhodamine B was used as a model drug in this study. V_2 phase gels were prepared by hydrating monoolein with rhodamine B stock solution in LB in a 70:30 ratio (m/v) using centrifugation. Briefly, monoolein was transferred to a centrifuge tube, followed by dye solution. The mixture was centrifuged (14 800 rpm; 10 min), mixed with a spatula, and this process repeated until homogenous. Dye-loaded gels were equilibrated at 37 ℃ for 16 h before transferring to individual minibeakers to simulate release from a single-sided matrix (cross-sectional area: 0.532 cm^2). The release matrices were stored at 37 ℃ prior to use.

In vitro release was conducted in triplicate using sealed dialysis bags to contain the bacterial subcultures. Briefly, dialysis tubing was sealed at one end, and to this was added: 2 mL of sterile LB (control); or 2 mL of *S. aureus* subculture in the exponential phase of growth. A filled minibeaker was added to each bag, the ends were tied, sterilised with 70 % ethanol (v/v), and transferred to a Schott bottle (250 mL) containing 200 mL sink volume (LB). Replicates were incubated at 37 ℃ with 180 rpm shaking for 50 h (Eppendorf, Innova 44 New Brunswick). Dye release over time was quantified by taking 1 mL samples of sink volume every 15 min for 1 h, then every 30 min for the following 6 hr. Subsequent samples were taken intermittently for two weeks. Sink volume was maintained by replenishing with 1 mL sterile LB after taking samples.

To ensure sterility in the samples taken from the sink volume, samples were flash-frozen in liquid nitrogen and subsequently thawed in a hot water bath (60 ℃) to lyse any bacterial cells. This was performed three times. Cell fragments were removed by centrifugation (14 800 rpm, 3 min), and the supernatant transferred to a 96-well plate for fluorescence measurement within an hour to prevent interference by further bacterial growth (BMG Labtech, CLARIOstar Plus).

2.5.3. Data analysis

Release of rhodamine B dye was used as a model for release of a hydrophilic drug from the lipid cubic phase.

Following previous work [38], the data obtained for the control experiments were fitted according to the following formula, based on standard Fickian diffusion

$$Q_{rel}(t) = 1 - \frac{8}{\pi^2}\sum_{n=0}^{\infty}\frac{1}{(2n+1)^2}e^{-(2n+1)^2\pi^2\frac{Dt}{4L^2}} \quad (4)$$

where $Q_{rel}(t)$ is the fraction of dye released at time t, D is the diffusion coefficient (corresponding to D_c or D_h depending on whether the symmetry is cubic or hexagonal), and $L = 0.3$ cm is the length of the minibeaker. Note that, compared to ref. [38], the formula has been adapted to account for the presence of a single release interface at the top of the minibeaker [39]. Errors in the fitting parameters were estimated following the iterative procedure described in ref. [40] by considering 2000 iterations.

In the case of release profiles in the presence of bacteria, we coupled the diffusion of the dye with the diffusion of the digested lipids. The lipids were characterized by Fickian diffusion with diffusion coefficient D_{dig}:

$$\frac{\partial w}{\partial t} = D_{dig}\frac{\partial^2 w}{\partial z^2} \quad (5)$$

where $w(z,t)$ is the fraction of digested lipids at position z and time t. Assuming lipid diffusion to be much slower than the digestion process, and that the latter takes place at the exposed face of the beaker, we can couple the previous diffusion equation with the boundary conditions $w(0,t) = 1, \frac{\partial w}{\partial z}(L,t) = 0$. The first condition considers that in proximity of the exposed face the symmetry is fully hexagonal at any time; the second condition implements a reflecting wall at the other end of the minibeaker. Moreover, we further consider the initial condition $w(z,0) = 0$, since there is only cubic symmetry at the beginning of the experiment. The numerical value for D_{dig} was obtained by analysing the growth rate k of hexagonal phases within a thin film under polarized light. The obtained rate was $k = (36.1 \pm 1.7)\text{Å}\cdot10^{-8}$ cm^2/s. This rate gives the area increase per unit time, i.e., $k = \frac{dA}{dt} = \pi\frac{d}{dt}r^2$, where the phase is assumed to have a circular section of radius r. Assuming a diffusing front and identifying r with the typical length obtained by the mean-square displacement of the digested lipids, we obtain $r^2 = 4D_{dig}t$, hence $D_{dig} = \frac{k}{4\pi} = (2.87 \pm 0.14)\text{Å}\cdot10^{-8}$ cm^2/s.

Based on the computed profile for $w(z,t)$, we then consider for the dye an effective diffusion coefficient D_{bac} equal to $D_{bac}(z,t) = w(z,t)D_h + (1 - w(z,t))D_c$. Then, D_{bac} is plugged into a diffusion equation with position- and time-dependent diffusion coefficient:

$$\frac{\partial c}{\partial t} = \frac{\partial}{\partial z}\left(D_{bac}\frac{\partial c}{\partial z}\right) \quad (6)$$

where c is the concentration profile of the dye. By treating the open and closed faces of the beaker respectively as an adsorbing and reflecting wall, the boundary conditions are $c(0,t) = 0, \frac{\partial c}{\partial z}(L,t) = 0$; moreover, the initial condition is $c(z,0) = c_0$, where c_0 is the concentration of dye initially loaded in the mesophase. Finally, the released amount of dye is computed as

$$Q_{rel}(t) = 1 - \frac{1}{c_0 L}\int_0^L c(z,t)dz \quad (7)$$

This coupled diffusion problem was solved numerically by considering standard discretization techniques [41]. Finally, the total fraction of hexagonal phase was computed as $\frac{1}{L}\int_0^L w(z,t)dz$.

3. Results and discussion

3.1. Effect of microbial strains on monoolein liquid crystal phase behaviour

Lipid nanoparticles were prepared by probe sonication of the constituent lipids and a sterile solution of Pluronic F-127 in the appropriate culturing media. The pH of lipid dispersions varied according to the lipid composition and type of culturing media used as this was necessary for the normal growth of bacterial strains; as such, the pH was monitored rather than buffered and considered during analysis (Table S1). The structured lipid particles were 100–300 nm in diameter with a moderate size distribution (Table S2).

To investigate the effect of representative bacterial strains on the dispersed lipidic particles, cubosomes were combined with inoculated culturing media and incubated overnight at physiological temperature. Control experiments employing sterile culturing media provide a reference for sterile conditions. Structural characterisation of the lipid mesophases was performed using small-angle X-ray scattering (SAXS) (Fig. 2). For monoolein cubosomes, the observation of Bragg peaks with q-spacing ratio $\sqrt{2}:\sqrt{4}:\sqrt{6}$ confirm the cubic (V_2; Im3m) structure in both types of sterile media (Fig. 2a). A clear transition in Bragg peaks is observed when exposed to *Staphylococcus aureus*; the resulting q-spacing ratio $\sqrt{1}:\sqrt{3}:\sqrt{4}$ is consistent with transition to H_2 structure. For monoolein hexosomes (Fig. 2b), the liquid crystalline structure remained unchanged after exposure to all bacterial strains except for *S. aureus*, which induced a clear transformation to inverse micellar cubic phase (I_2; Fd3m) (Table S3). No significant changes in lattice parameter were observed for cubosomes and hexosomes after exposure to all other representative bacteria (Table S3).

A follow up experiment was conducted for bulk, gel-like mesophases. The bulk MO bicontinuous cubic phase (V_2; Pn3m) in an excess of aqueous media produced similar results (Fig. 2c; see Fig. S1 for sample schematic): A partial transformation to hexagonal phase was observed after incubation with *S. aureus*; the cubic structure (Pn3m: $\sqrt{2}:\sqrt{3}:\sqrt{4}:\sqrt{6}:\sqrt{8}:\sqrt{9}$) was retained after exposure to all other bacterial strains. Additionally, upon inclusion of bacteria, no significant changes in cubic lattice parameter were observed (Table S4). These results demonstrate that the structural effects induced by *S. aureus* affect both dispersed and bulk liquid crystalline materials.

While pH is known to have pronounced effects on the phase behaviour of MO/OA/H_2O systems, it did not account for the phase changes induced by *S. aureus* (Table S1) [42]. There are two other possible mechanisms for these $V_2 \rightarrow H_2$ and $H_2 \rightarrow I_2$ transformations: modification of monoolein headgroups, or the transfer of lipids from bacterial cell membranes into the nanostructured lipid matrix. The enzymatic hydrolysis of monoolein, and subsequent accumulation of oleic acid in the lipid matrix, is known to cause transformation to more negatively-curved bilayer structures [28,29,43–45]. Indeed, *S. aureus* is well-known to express extracellular lipases [46], and monoolein systems undergo the transformation sequence $V_2 \rightarrow H_2 \rightarrow I_2$ as oleic acid content increases [33]. On the other hand, bacterial cell membranes are abundant in lipids known to cause structural transformations in monoolein systems. Phosphatidylethanolamine – the predominant cell membrane lipid in *E. coli* [47,48] – promotes negative bilayer curvature and $V_2 \rightarrow H_2$ transformation in monoolein systems at >35 wt% [49]. Phosphatidylglycerol – the predominant cell membrane lipid in *S. aureus* [47,50] – promotes lamellar (Lα) formation at > 50 wt% [51]. Cardiolipin – a minor constituent lipid in all bacteria studied [47,48] – promotes Lα formation at >30 wt% and significant lattice swelling (30–50 Å) at <1 wt% [49]. The remaining rich variety of lipid species found in bacterial cell membranes have not been studied with regards to effect on monoolein phase behaviour, nor the behaviour of any phospholipids on monoolein/oleic acid systems. Thus, characterizing the influence of this complete range of bacterial cell membrane lipids found *in vivo* was necessary to delineate the mechanism driving these structural transformations.

3.2. Exploring the mechanism driving structural transformation

To characterize the effect of bacterial cell membrane lipid transfer on monoolein phase behaviour, cubosomes were mixed with a nanoparticle dispersion of lipids isolated from *E. coli* cells [34]. Cubosomes were employed to overcome experimental and practical challenges of using

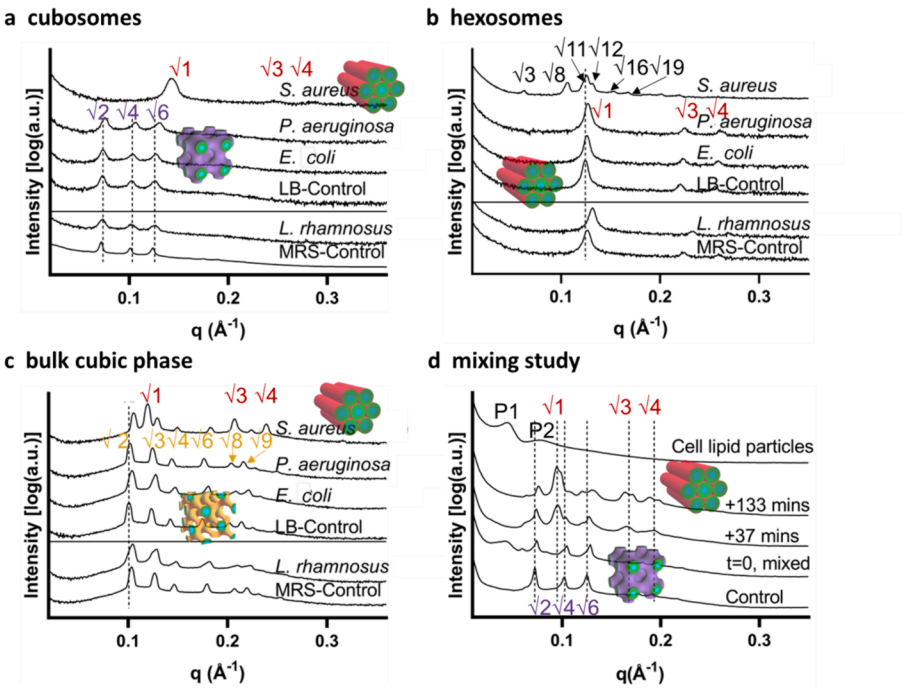

Fig. 2. Initial investigation of effects of live bacteria **(a–c)** and bacterial cell membrane components **(d)** on nanostructure. **(a–c)** SAXS patterns of monoolein nanostructured materials after equilibration with microbiome representatives and their respective culturing media (LB, MRS; sterile control); patterns acquired in different media are separated by a line. **(a)** cubosomes (Im3m; $\sqrt{2}$, $\sqrt{4}$, $\sqrt{6}$), **(b)** hexosomes (H_2: $\sqrt{1}$, $\sqrt{3}$, $\sqrt{4}$), and **(c)** bulk cubic phase (Pn3m: $\sqrt{2}$, $\sqrt{3}$, $\sqrt{4}$, $\sqrt{6}$, $\sqrt{8}$, $\sqrt{9}$) retain their native liquid crystal structure in sterile media after exposure to all bacteria except for *S. aureus*, which demonstrates a transition to the inverse hexagonal (H_2: $\sqrt{1}$, $\sqrt{3}$, $\sqrt{4}$), inverse micellar cubic (Fd3m: $\sqrt{3}$, $\sqrt{8}$, $\sqrt{11}$, $\sqrt{12}$, $\sqrt{16}$…) and inverse hexagonal (H_2: $\sqrt{1}$, $\sqrt{3}$, $\sqrt{4}$) phase, respectively. **(d)** Time-resolved synchrotron SAXS patterns of monoolein cubosomes during mixing with cell lipid particles. Particles composed of lipids isolated from *E. coli* cell membranes (top) are characterised by two broad peaks ***P1* & *P2*,** while Im3m cubosomes (bottom) are characterised by Bragg peaks with spacing $\sqrt{2}$, $\sqrt{4}$, $\sqrt{6}$. The development of peaks with spacing $\sqrt{1}$, $\sqrt{3}$, $\sqrt{4}$ throughout mixing signifies the formation of two distinct H_2 phases with different lattice parameters. The loss of the broad bump ***P1*** throughout mixing signifies lipid transfer between the two particle populations.

bulk phases; the behaviour of cubosomes translates to that of the bulk material given that liquid crystal structure is maintained internally within the nanoparticle, while the surface layer of polymeric steric stabilizer does not prevent inter-particle lipid exchange [52,53]. Dynamic structural characterisation was observed using synchrotron SAXS. The lipid formulations used in the dynamic synchrotron study had approximately the same pH (within 0.2 units) and the structured lipid particles were on the order of 300 nm in diameter with a moderate size distribution (Table S5).

SAXS diffraction patterns acquired before and after mixing with extracted cell membrane lipid particles illustrate the behaviour of the system over time (Fig. 2d). The loss of the two broad peaks characteristic of the cell membrane lipid particles (*P*1, *P*2) signals a loss of its original structure and suggests lipid transfer. This is accompanied by the formation of two distinct H_2 structures, both with lattice parameters ~75 Å, characterized by Bragg peaks with q-spacing ratio ($\sqrt{1}$:$\sqrt{3}$:$\sqrt{4}$) (Table S6). This is a significantly larger lattice parameter than the H_2 phase formed after exposure to *S. aureus* (~51 Å) and in the case of sterile monoolein hexosomes (~55 Å). Together, these alterations are consistent with transfer of bacterial phospholipids into the cubosomes matrix, with phase transformations consistent with transfer of the predominant membrane lipid, phosphatidylethanolamine, and lattice swelling consistent with transfer of cardiolipin [48].

In order to delineate the mechanism driving these structural transformations, the effect of other biological macromolecules and colloids on monoolein phase behaviour was investigated. Cultures of *S. aureus* and *E. coli* were separated by centrifugal ultrafiltration into cell membrane/extracellular vesicle (EV), free-protein, and peptide/ion fractions (10–450 nm, 1–10 nm, & <1 nm, respectively). Monoolein cubosomes were exposed to each fraction analogous to treatment with live cultures, followed by structural identification using SAXS (Fig. 3).

No phase changes were observed after treatment with any *E. coli* fractions (Fig. 3a). Given that a transformation to H_2 phase would be consistent with enrichment in PE, the main lipid in bacterial cell membranes [48,49], this further supports the notion that lipid transfer in the context of live bacterial exposure has negligible effects on monoolein phase behaviour. Indeed, no significant lattice swelling was observed after exposure with the cell membrane/EV fraction, nor with any live microbiome strain (Table S9).

Together, this suggests that lipid transfer from live bacteria to lipid mesophases does not occur to a significant extent. This lack of transfer appears to be generalized across gram-negative and gram-positive strains and may be attributed to the bacterial glycocalyx acting as a barrier and preventing lipid transfer, or insufficient quantities of lipid being present to achieve the percentages required for phase transformation to occur [54,55].

Different phase changes were observed after treatment with different *S. aureus* size class fractions (Fig. 3b). Treatment with the free-protein fraction caused transformation to H_2, while treatment with the cell membrane/EV fraction caused a transformation to I_2. Given that the extracellular lipases are secreted in EVs by *S. aureus*, lipase is most concentrated in EVs; smaller amounts are free in solution as a fraction of EVs deterioration/disintegration over time [56]. Consequently, the $V_2 \rightarrow H_2$ and $V_2 \rightarrow I_2$ transformations observed with free-protein and cell membrane/EV fractions are consistent with less extensive and more extensive enzymatic hydrolysis, respectively [28,42]. Furthermore, these phase transitions are inconsistent with PG enrichment – which would lead to transformation to Lα phase.

Accordingly, we thus conclude that the structural transformations induced by live *S. aureus* are unlikely to be mediated by a lipid transfer mechanism. These results strongly support the mechanism proceeding via the action of *Staphylococcal* lipases.

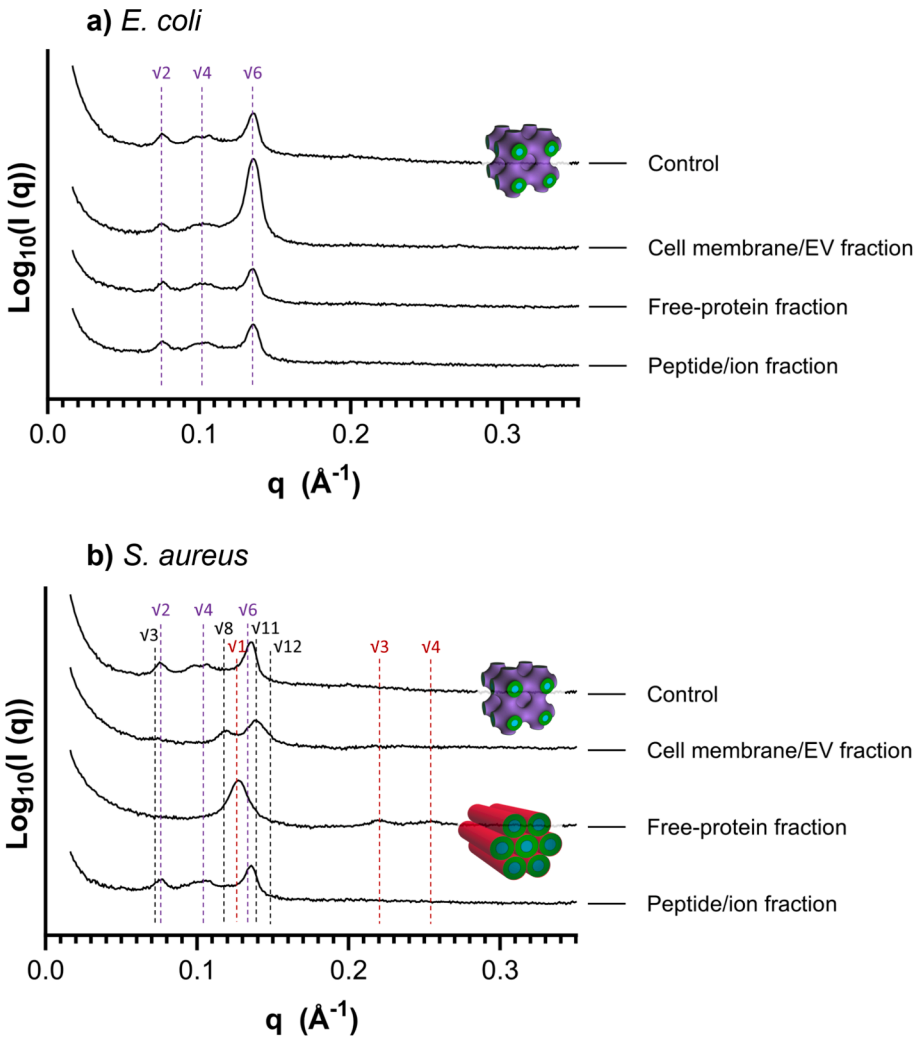

Fig. 3. SAXS diffraction patterns for monoolein cubosomes (control; Im3m: $\sqrt{2}$, $\sqrt{4}$, $\sqrt{6}$)) after overnight incubation with different size class fractions separated from cultures of **(a)** *E. coli* and **(b)** *S. aureus*. **a)** Treatment with any fraction caused no observable changes. **b)** Treatment with the cell membrane/EV fraction (10–450 nm) caused a transformation to inverse micellar cubic phase (Fd3m: $\sqrt{3}$, $\sqrt{8}$, $\sqrt{11}$, $\sqrt{12}$…), while the free-protein fraction (1–10 nm) caused a transformation to the inverse hexagonal phase (H_2: $\sqrt{1}$, $\sqrt{3}$, $\sqrt{4}$). Treatment with the peptide/ion fraction (<1 nm) caused no observable change.

3.3. Exploration of kinetics and effect on drug release

The effect of overnight incubation with *S. aureus* on the bulk monoolein mesophase was observed with polarised light microscopy (Fig. 4, Fig. S2). The transition $V_2 \rightarrow H_2$ is identified by the formation of fan-like birefringent structures under cross-polarized light [37]. Sterile monoolein gels (Fig. S3) and *S. aureus* subculture alone (Fig. S4) did not display this transformation over the same time interval. A timelapse of the representative sample is provided as supplementary information (Movie 1), where the structural change is observed to spread out from central seed points (see Fig. 4).

Analysis of the growth clusters in the timelapse revealed that transformation commenced after ~8 hr of exposure, originated from central loci and spread radially throughout the gel at a rate of 36.1 ± 1.7 $\mu m^2/s$ (mean $\pm$ σ, $n = 3$).

Dye-loaded monoolein nanostructured gels were employed in release studies to investigate the effect of this structural transformation on drug release properties. SAXS data is included as SI (Figs. S5, S6, Table S10).

To gain a quantitative understanding of the release profiles, we considered a diffusion model in which the dye is transported through the minibeaker (Schematic: Fig. S7) according to an effective diffusion coefficient, which quantitatively depends on the nanoscopic features of the mesophase. For the control mesophases, this parameter can be obtained by fitting the release profiles according to a formula based on standard Fickian diffusion (Equation (4), yielding $D_c = (3.49 \pm 0.08)\text{Å}\cdot10^{-8}$ cm^2/s and $D_h = (0.52 \pm 0.05)\text{Å}\cdot10^{-8}$ cm^2/s for cubic and hexagonal phases, respectively (see golden stars, red circles and dotted curves in Fig. 5). This ~7-fold difference has been similarly observed between V_2 and H_2 phases [57]. In the presence of bacteria, the hydrolysis of monoolein results in a heterogeneous composition of mesophases, which gradually tune their nanoscopic arrangement from V_2 to H_2 over the course of the release process. Moreover, since hydrolysis takes place at the exposed face of the minibeaker, there may be a gradient of concentration of the resulting oleic acid which decreases further from the exposed face at any time; this results in space-dependent relative populations of hexagonal and cubic phases.

Quantitatively, we assume that the effective diffusion coefficient of the dye in the presence of bacteria, D_{bac}, is dependent on the distance, z, from the exposed face and on the time, t, elapsed since the start of the digestion process (assumed to be simultaneous to the beginning of the release). This dependence on space and time is accounted for by $D_{bac} = wD_h + (1-w)D_c$, where $w(z,t)$ is the fraction of digested lipids at position z and at time t. The profile of $w(z,t)$ can be obtained by considering Fickian diffusion also for the digested lipids, where a boundary condition $w(0,t) = 1$ is imposed by assuming lipid diffusion to be much slower than digestion (see Methods for further details). Within this

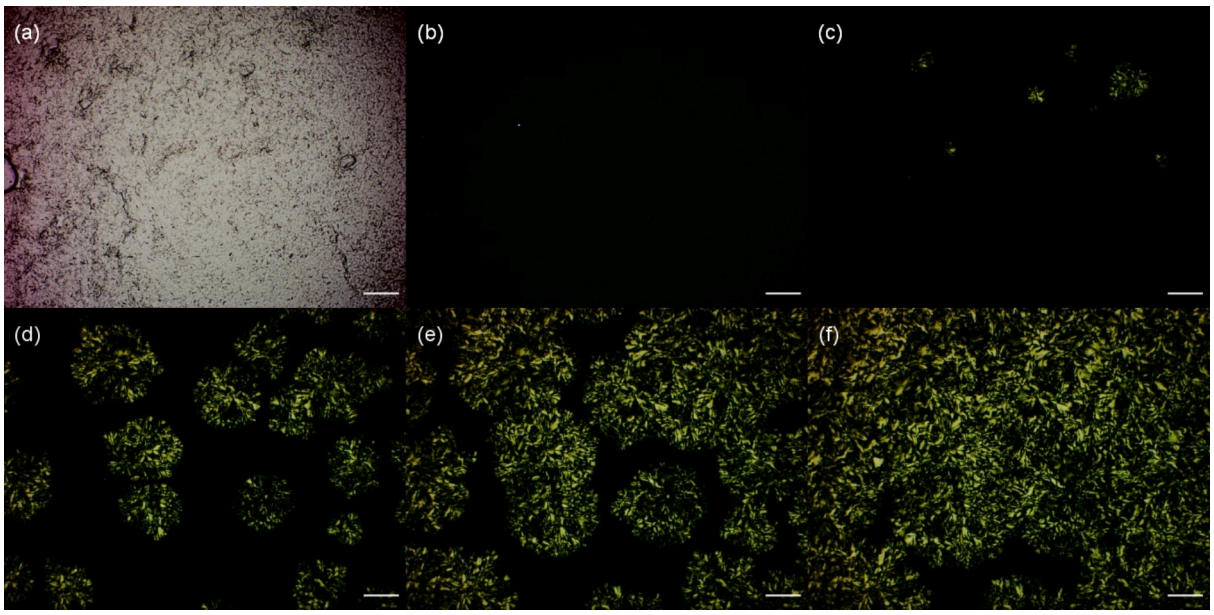

Fig. 4. Timelapse images from Movie 1 (SI): Bright-field **(a)** and polarized light **(b)** images of the bulk mesophase at t = 0. Subsequent polarized light images **(c → f)** at t = 8.5, 10, 12 and 14 hr illustrate the $V_2 \rightarrow H_2$ phase change. Scale bars = 100 μm.

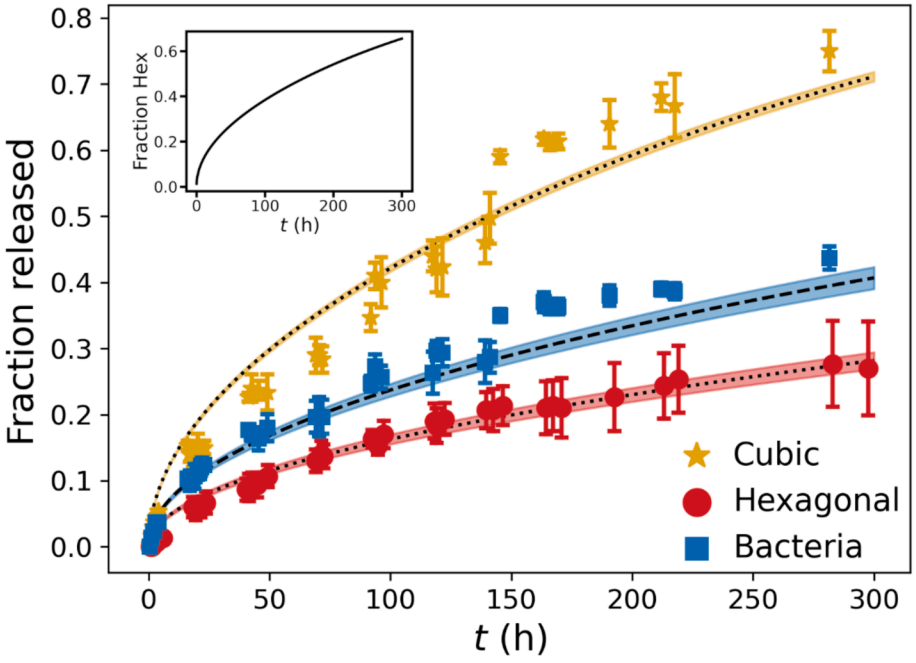

Fig. 5. Release profiles in the absence of bacteria for bicontinuous cubic (golden stars) and inverse hexagonal (red circles) phases, and release data in the presence of bacteria (blue squares). Dotted lines are the fits obtained by tuning D_c and D_h in the theoretical formula reported in the Methods. The dashed line is the prediction for the release obtained by solving the coupled diffusion problem. Note that all the parameters used to compute the dashed line were obtained via control experiments, i.e. this prediction is not the result of a fitting procedure. Shaded areas indicate the indeterminacy associated to the error of the parameters. In the inset, we plot the time evolution of the overall fraction of the inverse hexagonal structure within the mesophase in the presence of bacteria. (For interpretation of the references to colour in this figure legend, the reader is referred to the web version of this article.)

approach, $w(z,t)$ can be computed by knowing the diffusion coefficient of the digested lipids, D_{dig}, which we estimated to be $D_{dig} = (2.87 \pm 0.14)\text{Å}\cdot 10^{-8}$ cm^2/s based on the growth rate of hexagonal mesophases in thin films as measured by polarized light microscopy (Fig. 3, 36.1 ± 1.7 μm^2/s). In Fig. 5, we report the predicted release profile as a dashed line against the experimental data (blue squares). The excellent quantitative agreement strongly supports our microscopic model, particularly considering that all parameters used for computation were derived from control experiments. An insightful byproduct of the calculation is provided in the inset of Fig. 5, where we report the time evolution of the overall fraction of mesophase with hexagonal symmetry, as estimated from our model. It can be appreciated that the nanoscopic change in the structure occurs at comparable times as the release process, which is a direct consequence of the similar magnitude between D_{dig} and D_{bac}. As can be seen, release of encapsulated hydrophilic molecules in the presence of *S. aureus* is a balance between

the rate of bacterial growth, lipid diffusion, and consequent lipid mesophase structure transformation.

4. Conclusions

Towards the development of nanostructured lipidic drug delivery systems, this study has investigated the effect of representative strains of live bacteria found in the human microbiome on these materials. As these materials are formed by the self-assembly of polar lipids in aqueous conditions, their intermolecular arrangement is affected by changes in solution conditions – including changes resulting from microbial growth. This study demonstrates that monoolein-based lipid mesophases are susceptible to transformation from $V_2 \rightarrow H_2 \rightarrow I_2$ structures when exposed to live bacteria commonly found on the skin and nasal mucosa (*S. aureus*). The transformation has been attributed to enzyme-mediated hydrolysis taking place within an application-relevant timeframe (~8 h), which significantly reduces the rate of drug release. Given that lipase secretion is a common adaptation for overcoming low nutrient availability in the skin biome, this transformation could be elicited by members of the skin biome in general [6]. These findings will inform the future development of these materials for transdermal applications.

Structural transformations also occurred upon mixing the lipidic particles with the polar lipids extracted from bacterial cell membranes. This is hypothesised to have a similar effect on drug release, and PEGylated surface stabilisers on cubosomes did not prevent this effect. While no evidence for lipid transfer was observed when exposed to live bacteria, it is thought that the cell fragments and debris constantly being shed as bacteria die may cause a similar effect. This effect might cause changes in lipid behaviour in applications where the lipidic formulations are exposed to large concentration of these fragments during residence time, for example in the case of suppository formulations.

In conclusion, our results show that the human microbiome produces physiological stimuli that can alter the drug delivery capacity of lipidic carriers. These results suggest that the presence of the human microbiome and its interaction with lipidic nanomaterials should be taken into consideration in the designing of drug formulations or therapeutic agents. This aspect will be particularly important for the successful creation of lipidic carriers for the treatment of bacterial infections, where bacterial concentrations can be much higher than in normal physiological fluids [18]. Moreover, the intrinsic differences in microbiome population from body region to body region and from patient to patient can be exploited to tune selectivity in drug release, or towards the development of personalised medicine [6,8].

CRediT authorship contribution statement

Jonathan Caukwell: Writing – review & editing, Writing – original draft, Methodology, Investigation, Formal analysis, Data curation. **Salvatore Assenza:** Visualization, Validation, Formal analysis. **Karl A. Hassan:** Writing – review & editing, Supervision, Methodology. **Brett A. Neilan:** Supervision, Resources, Methodology. **Andrew J. Clulow:** Writing – review & editing, Supervision, Methodology, Data curation. **Livia Salvati Manni:** Writing – review & editing, Writing – original draft, Supervision, Methodology, Investigation, Data curation, Conceptualization. **Wye-Khay Fong:** Writing – review & editing, Supervision, Resources, Project administration, Funding acquisition, Data curation, Conceptualization.

Declaration of Competing Interest

The authors declare the following financial interests/personal relationships which may be considered as potential competing interests: Wye-Khay Fong reports financial support was provided by Noxopharm Limited. Jonathan Caukwell reports financial support was provided by Australian Nuclear Science and Technology Organisation. Salvatore Assenza reports financial support was provided by LaCaixa Foundation. Salvatore Assenza reports financial support was provided by European Commission Marie Sklodowska-Curie Actions. Salvatore Assenza reports financial support was provided by Spanish Scientific Research Council. Livia Salvati Manni reports financial support was provided by Swiss National Science Foundation. Karl Hassan, Brett Neilan reports financial support was provided by Australian Research Council. If there are other authors, they declare that they have no known competing financial interests or personal relationships that could have appeared to influence the work reported in this paper.

Data availability

Data will be made available on request.

Acknowledgements

The authors acknowledge: Jesse Cain, Daniel Nebauer, Alescia Cullen, and Joachim Larsen for scientific discussions; Frithjof Herb for his experimental assistance; Sydney Analytical for access to their SAXS instrument and Paul A. Fitzgerald for his experimental assistance; the use of facilities within the Monash X-ray Platform (MXP); the expertise and assistance of Nigel Kirby, Claire Scott, and Kirsty Brunt during time-resolved SAXS experiments conducted on the SAXS/WAXS beamline of the Australian Synchrotron, ANSTO, Australia. J.C. received support of a scholarship and funding through the ANSTO Future Now program. L.S.M. acknowledges the Swiss National Foundation of Science for financial support grant no. P2ZHP2_187769. S.A. received the support of a fellowship from “la Caixa” Foundation (ID 100010434) and from the European Union’s Horizon research and innovation programme under the Marie Skłodowska-Curie grant agreement No. 847648. The fellowship code is LCF/BQ/PI20/11760019. S.A. acknowledges support from MCIN/AEI/10.13039/501100011033 and FSE+through a Ramón y Cajal Fellowship (ref. RYC2022-037744-I).

Appendix A. Supplementary data

Supplementary data to this article can be found online at https://doi.org/10.1016/j.jcis.2024.07.216.

References

[1] A. Yaghmur, H. Mu, Recent advances in drug delivery applications of cubosomes, hexosomes, and solid lipid nanoparticles, Acta Pharm. Sin. B 11 (2021) 871–885, https://doi.org/10.1016/j.apsb.2021.02.013.
[2] J.Y.T. Chong, X. Mulet, B.J. Boyd, C.J. Drummond, Steric stabilizers for cubic phase lyotropic liquid crystal nanodispersions (cubosomes), in: Adv Planar Lipid Bilayers Liposomes, first ed., Academic Press, 2015, pp. 131–187, https://doi.org/10.1016/bs.adplan.2014.11.001.
[3] M.P. Monopoli, C. Åberg, A. Salvati, K.A. Dawson, Biomolecular coronas provide the biological identity of nanosized materials, Nat Nanotechnol. 7 (2012) 779–786, https://doi.org/10.1038/nnano.2012.207.
[4] S. Ritz, S. Schöttler, N. Kotman, et al., Protein corona of nanoparticles: distinct proteins regulate the cellular uptake, Biomacromolecules 16 (2015) 1311–1321, https://doi.org/10.1021/acs.biomac.5b00108.
[5] D. Knight, K. Girling, Gut flora in health and disease, Lancet 361 (2003) P1831, https://doi.org/10.1016/S0140-6736(03)13438-1.
[6] A.L. Byrd, Y. Belkaid, J.A. Segre, The human skin microbiome, Nat. Rev. Microbiol. 16 (2018) 143–155, https://doi.org/10.1038/nrmicro.2017.157.
[7] L.K. Ursell, J.L. Metcalf, L.W. Parfrey, R. Knight, Defining the human microbiome, Nutr. Rev. 70 (2012) S38–S44, https://doi.org/10.1111/j.1753-4887.2012.00493.x.
[8] E. Thursby, N. Juge, Introduction to the human gut microbiota, Biochem. J. 474 (2017) 1823–1836, https://doi.org/10.1042/BCJ20160510.
[9] M. Zimmermann, M. Zimmermann-Kogadeeva, R. Wegmann, A.L. Goodman, Mapping human microbiome drug metabolism by gut bacteria and their genes, Nature 570 (2019) 462–467, https://doi.org/10.1038/s41586-019-1291-3.
[10] M. Klünemann, S. Andrejev, S. Blasche, et al., Bioaccumulation of therapeutic drugs by human gut bacteria, Nature 597 (2021) 533–538, https://doi.org/10.1038/s41586-021-03891-8.
[11] S. Phan, W.K. Fong, N. Kirby, et al., Evaluating the link between self-assembled mesophase structure and drug release, Int. J. Pharm. 421 (2011) 176–182, https://doi.org/10.1016/j.ijpharm.2011.09.022.

[12] A.M. Bosch, S. Assenza, Interplay of hydropathy and heterogeneous diffusion in the molecular transport within lamellar lipid mesophases, Pharmaceutics 15 (2023) 573, https://doi.org/10.3390/pharmaceutics15020573.
[13] J. Gustafsson, H. Ljusberg-Wahren, M. Almgren, K. Larsson, Cubic lipid−water phase dispersed into submicron particles, Langmuir 12 (1996) 4611–4613, https://doi.org/10.1021/la960318y.
[14] X. Mulet, B.J. Boyd, C.J. Drummond, Advances in drug delivery and medical imaging using colloidal lyotropic liquid crystalline dispersions, J. Colloid Interface Sci. 393 (2013) 1–20, https://doi.org/10.1016/j.jcis.2012.10.014.
[15] R. Negrini, W.K. Fong, B.J. Boyd, R. Mezzenga, PH-responsive lyotropic liquid crystals and their potential therapeutic role in cancer treatment, Chem. Commun. 51 (2015) 6671–6674, https://doi.org/10.1039/c4cc10274f.
[16] C.J.H. Porter, N.L. Trevaskis, W.N. Charman, Lipids and lipid-based formulations: optimizing the oral delivery of lipophilic drugs, Nat. Rev. Drug. Discov. 6 (2007) 231–248, https://doi.org/10.1038/nrd2197.
[17] W.K. Fong, R. Negrini, J.J. Vallooran, et al., Responsive self-assembled nanostructured lipid systems for drug delivery and diagnostics, J. Colloid Interf. Sci. 484 (2016) 320–339, https://doi.org/10.1016/j.jcis.2016.08.077.
[18] C.R. Thorn, N. Thomas, B.J. Boyd, C.A. Prestidge, Nano-fats for bugs: the benefits of lipid nanoparticles for antimicrobial therapy, Drug Deliv. Transl. Res. 11 (2021) 1598–1624, https://doi.org/10.1007/s13346-021-00921-w.
[19] C.R. Thorn, Z. Kopecki, A. Wignall, et al., Liquid crystal nanoparticle platform for increased efficacy of cationic antimicrobials against biofilm infections, Nanomedicine 42 (2022), https://doi.org/10.1016/j.nano.2022.102536.
[20] C.R. Thorn, D. Raju, I. Lacdao, et al., Protective liquid crystal nanoparticles for targeted delivery of PslG: a biofilm dispersing enzyme, ACS Infect. Dis. 7 (2021) 2102–2115, https://doi.org/10.1021/acsinfecdis.1c00014.
[21] C.R. Thorn, C. de S. Carvalho-Wodarz, J.C. Horstmann, et al., Tobramycin liquid crystal nanoparticles eradicate cystic fibrosis-related pseudomonas aeruginosa biofilms, Small 17 (2021), https://doi.org/10.1002/smll.202100531.
[22] C.R. Thorn, C.A. Prestidge, B.J. Boyd, N. Thomas, Pseudomonas infection responsive liquid crystals for glycoside hydrolase and antibiotic combination, ACS Appl. Bio Mater. 1 (2018) 281–288, https://doi.org/10.1021/acsabm.8b00062.
[23] L. Boge, K. Hallstensson, L. Ringstad, et al., Cubosomes for topical delivery of the antimicrobial peptide LL-37, Eur. J. Pharm. Biopharm. 134 (2019) 60–67, https://doi.org/10.1016/j.ejpb.2018.11.009.
[24] T.G. Meikle, B.P. Dyett, J.B. Strachan, et al., Preparation, characterization, and antimicrobial activity of cubosome encapsulated metal nanocrystals, ACS Appl. Mater. Interf. 12 (2020) 6944–6954, https://doi.org/10.1021/acsami.9b21783.
[25] B.P. Dyett, H. Yu, J. Strachan, et al., Fusion dynamics of cubosome nanocarriers with model cell membranes, Nat. Commun. 10 (2019), https://doi.org/10.1038/s41467-019-12508-8.
[26] B.P. Dyett, H. Yu, S. Sarkar, et al., Uptake dynamics of cubosome nanocarriers at bacterial surfaces and the routes for cargo internalization, ACS Appl. Mater. Interf. 13 (2021) 53530–53540, https://doi.org/10.1021/acsami.1c09909.
[27] S. Aleandri, R. Mezzenga, The physics of lipidic mesophase delivery systems, Phys. Today 73 (2020) 38–44, https://doi.org/10.1063/PT.3.4522.
[28] L. Salvati Manni, M. Duss, S. Assenza, et al., Enzymatic hydrolysis of monoacylglycerols and their cyclopropanated derivatives: molecular structure and nanostructure determine the rate of digestion, J. Colloid Interface Sci. 588 (2021) 767–775, https://doi.org/10.1016/j.jcis.2020.11.110.
[29] J. Borné, T. Nylander, A. Khan, Effect of lipase on monoolein-based cubic phase dispersion (cubosomes) and vesicles, J. Phys. Chem. B 106 (2002) 10492–10500, https://doi.org/10.1021/jp021023y.
[30] M. Dully, C. Brasnett, A. Djeghader, et al., Modulating the release of pharmaceuticals from lipid cubic phases using a lipase inhibitor, J. Colloid Interf. Sci. 573 (2020) 176–192, https://doi.org/10.1016/j.jcis.2020.04.015.
[31] C.R. Thorn, A.J. Clulow, B.J. Boyd, et al., Bacterial lipase triggers the release of antibiotics from digestible liquid crystal nanoparticles, J. Control. Release 319 (2020) 168–182, https://doi.org/10.1016/j.jconrel.2019.12.037.
[32] B. Sommer, D.P. Overy, B. Haltli, R.G. Kerr, Secreted lipases from Malassezia globosa: recombinant expression and determination of their substrate specificities, (n.d.). doi: 10.1099/mic.0.000299.
[33] W. Yao, K. Liu, H. Liu, et al., A valuable product of microbial cell factories: microbial lipase, Front Microbiol. 12 (2021) 2724, https://doi.org/10.3389/FMICB.2021.743377/BIBTEX.
[34] W.J. Bligh, E.G. Dyer, A rapid method of total lipid extraction and purification, Can. J. Biochem. Physiol. 37 (1959) 911–917, https://doi.org/10.1139/o59-099.
[35] V. Cherezov, Crystallizing membrane proteins using lipidic mesophases, Nat. Protoc. 4 (2009) 706–731, https://doi.org/10.1038/nprot.2009.31.
[36] N.M. Kirby, S.T. Mudie, A.M. Hawley, et al., A low-background-intensity focusing small-angle X-ray scattering undulator beamline, J. Appl. Crystallogr. 46 (2013) 1670–1680, https://doi.org/10.1107/S002188981302774X.
[37] S.T. Hyde, Identification of lyotropic liquid crystalline mesophases, in: K. Holmberg (Ed.), Handbook of Applied Surface and Colloid Chemistry, John Wiley & Sons Ltd, 2001, pp. 299–332.
[38] L.M. Antognini, S. Assenza, C. Speziale, R. Mezzenga, Quantifying the transport properties of lipid mesophases by theoretical modelling of diffusion experiments, J. Chem. Phys. 145 (2016) 084903, https://doi.org/10.1063/1.4961224.
[39] J. Crank, The Mathematics of Diffusion, second ed., Oxford University Press, 1979 doi:10.1021/ja01562a072.
[40] S. Assenza, R. Pérez, Accurate sequence-dependent coarse-grained model for conformational and elastic properties of double-stranded DNA, J. Chem. Theory Comput. 18 (2022) 3239–3256, https://doi.org/10.1021/acs.jctc.2c00138.
[41] R. Ghanbari, S. Assenza, P. Zueblin, R. Mezzenga, Impact of molecular partitioning and partial equilibration on the estimation of diffusion coefficients from release experiments, Langmuir 35 (2019) 5663–5671, https://doi.org/10.1021/acs.langmuir.9b00510.
[42] S. Salentinig, L. Sagalowicz, O. Glatter, Self-assembled structures and pK a value of oleic acid in systems of biological relevance, Langmuir 26 (2010) 11670–11679, https://doi.org/10.1021/la101012a.
[43] J.L. Brennan, A.G. Kanaras, P. Nativo, et al., Enzymatic activity of lipase-nanoparticle conjugates and the digestion of lipid liquid crystalline assemblies, Langmuir 26 (2010) 13590–13599, https://doi.org/10.1021/la1018604.
[44] A.F. Hofmann, B. Borgström, Hydrolysis of long-chain monoglycerides in micellar solution by pancreatic lipase, in: Biochim. Biophys. Acta (BBA) Special. Sect. Lip. Related Subjects, 70, 1963, pp. 317–331, https://doi.org/10.1016/0926-6542(63)90044-1.
[45] S. Phan, S. Salentinig, A. Hawley, B.J. Boyd, Immobilised lipase for in vitro lipolysis experiments, J. Pharm. Sci. 104 (2015) 1311–1318, https://doi.org/10.1002/jps.24327.
[46] A. Lepidi, Staphylococcal lipases, in: Pet-to-Man Travelling Staphylococci: A World in Progress, Elsevier Inc., 2018, pp. 147–159. doi: 10.1016/B978-0-12-813547-1.00012-1.
[47] C. Sohlenkamp, O. Geiger, Bacterial membrane lipids: diversity in structures and pathways, FEMS Microbiol. Rev. 40 (2015) 133–159, https://doi.org/10.1093/femsre/fuv008.
[48] C.R.H. Raetz, W. Dowhan, Biosynthesis and function of phospholipids in *Escherichia coli*, J. Biol. Chem. 265 (1990) 1235–1238, https://doi.org/10.1016/s0021-9258(19)40001-x.
[49] V. Cherezov, J. Clogston, Y. Misquitta, et al., Membrane protein crystallization in meso: lipid type-tailoring of the cubic phase, Biophys. J. 83 (2002) 3393–3407, https://doi.org/10.1016/S0006-3495(02)75339-3.
[50] S.A. Young, A.P. Desbois, P.J. Coote, T. Smith, Characterisation of Staphylococcus aureus lipids by nanoelectrospray ionisation tandem mass spectrometry (nESI-MS/MS), BioRxiv (2019) 593483, https://doi.org/10.1101/593483.
[51] V. Chupin, J.A. Killian, B. De Kruijff, Effect of phospholipids and a transmembrane peptide on the stability of the cubic phase of monoolein: implication for protein crystalization from a cubic phase, Biophys. J. 84 (2003) 2373–2381, https://doi.org/10.1016/S0006-3495(03)75043-7.
[52] C. Moitzi, S. Guillot, G. Fritz, et al., Phase reorganization in self-assembled systems through interparticle material transfer, Adv. Mater. 19 (2007) 1352–1358, https://doi.org/10.1002/adma.200601679.
[53] A. Tilley, Y.-D. Da Dong, H. Amenitsch, et al., Transfer of lipid and phase reorganisation in self-assembled liquid crystal nanostructured particles based on phytantriol, PCCP 13 (2011) 3026–3032, https://doi.org/10.1039/c0cp01724h.
[54] J.W. Costerton, R.T. Irvin, K.J. Cheng, The bacterial glycocalyx in nature and disease, Annu. Rev. Microbiol. 35 (1981) 299–324, https://doi.org/10.1146/ANNUREV.MI.35.100181.001503/CITE/REFWORKS.
[55] T.J. Silhavy, D. Kahne, S. Walker, The bacterial cell envelope, Cold Spring Harb. Perspect. Biol. 2 (2010), https://doi.org/10.1101/CSHPERSPECT.A000414.
[56] E.Y. Lee, D.Y. Choi, D.K. Kim, et al., Gram-positive bacteria produce membrane vesicles: proteomics-based characterization of Staphylococcus aureus-derived membrane vesicles, Proteomics 9 (2009) 5425–5436, https://doi.org/10.1002/PMIC.200900338.
[57] W.K. Fong, T. Hanley, B.J. Boyd, Stimuli responsive liquid crystals provide "on-demand" drug delivery in vitro and in vivo, J. Control. Release 135 (2009) 218–226, https://doi.org/10.1016/j.jconrel.2009.01.009.